Coupling or decoupling bed and flow dynamics: Fast and slow sediment waves at high Froude numbers

Marco Colombini[a] and Alessandro Stocchino
Dipartimento di Ingegneria Ambientale, Università degli Studi di Genova, Via Montallegro 1, 16145 Genova, Italy

(Received 7 June 2004; accepted 5 November 2004; published online 4 February 2005)

The effect of coupling or decoupling bed and flow dynamics is analyzed in the framework of a linear analysis of the stability of a uniform, rotational, two-dimensional flow in an infinitely wide channel with a bed composed by incoherent sediments. It is shown that results obtained with the coupled analysis in term of instability of slow sediment waves of the dune/antidune kind are quite similar to the results obtained making use of the "quasisteady hypothesis," which forms the basis of most of the existing linear stability analyses of bedforms and formally justifies the decoupling procedure. Small differences can be observed, for Froude numbers of $O(1)$, in the surroundings of the marginal curves that bound the instability regions, mainly due to the removal of the artificial resonance that is introduced in the analysis when the quasisteady hypothesis is enforced. The decoupled approach, however, completely wipes out a mode of instability associated with fast-moving sediment waves, which appear at high Froude numbers in connection with the formation of roll waves on the free surface. This mode of instability, characterized by large wavelengths, is shown to coexist with the slower, shorter antidune mode. © *2005 American Institute of Physics*. [DOI: 10.1063/1.1848731]

I. INTRODUCTION

Starting from the seminal work of Kennedy,[1] stability analyses proved to be a powerful tool to investigate the formation mechanism of bedforms, represented as periodic sediment waves traveling upstream or downstream while amplifying in time.[2–8]

In a linear context, information is gathered about the existence of unstable regions in the parameter space and on the wavelength of the most unstable mode. A satisfactory agreement of the theoretical predictions with the experimental observations is found, thus confirming that the basic mechanism of bedform formation is indeed an instability mechanism, which is necessarily associated with the presence of a phase lag between sediment transport and bed topography. Nevertheless, criticism towards the latter approach has been leveled[9,10] regarding the way information coming from a linear theory, which assumes infinitesimal amplitude of the disturbances, can be transferred to the dynamics of finite amplitude bedforms. Indeed, a few weakly nonlinear stability theories[11–13] showed that, at least for some class of bedforms, finite amplitude solutions can be predicted with a sufficient degree of accuracy.

In the formulation of his work, Kennedy[1] also introduced the idea of decoupling bed and flow dynamics. This hypothesis was made under the realistic assumption that the bed evolves on a time scale that is much slower than the characteristic time scale of the flow. Following this approach, the problem can be decoupled, i.e., split into two parts: (i) the determination of the "forced" steady response of the flow to a given bottom perturbation; (ii) the determination of the time evolution of the bed driven by the latter flow response. The above assumption strongly simplifies the linear analysis, since the resulting eigenrelation is invariably linear, thus leading to the determination of just one eigenvalue associated with the amplification and propagation of bed perturbations. For its simplicity, this assumption was adopted in almost any subsequent linear stability analysis of bedforms. Nevertheless, the above hypothesis completely rules out any mode of instability associated with the flow, possibly leading to incomplete predictions.[4,10,14] The consequences of this choice become evident when the instability of the complete flow-bed system, which will be formally derived in the following, is analyzed. It suffices here to state that the above decoupling procedure produces an unrealistic resonant behavior in the region where quasisteady flow disturbances occur and the disappearance of a mode of instability associated to the formation of roll waves at high Froude numbers.

The main goal of the present contribution is to assess the role of flow unsteadiness (and thus of coupling or decoupling bed and flow dynamics) in the framework of a linear stability of a uniform flow in an infinitely wide open channel with erodible bed. This will be accomplished in the following by means of a direct comparison between the results of coupled and decoupled solutions obtained adopting the same flow model. A two-dimensional rotational flow model is employed, which provides a good description of the phase lag between flow and bed topography that drives the whole instability process. Only equilibrium bedload transport is considered and the analysis is therefore restricted to coarse sediments, neglecting the role of particle inertia.

The rest of the paper proceeds as follows. The differential system that governs the evolution of the flow-bed system is formulated in Sec. II and linearized in the following section where the resulting eigenvalue problem is obtained. Re-

[a]Author to whom correspondence should be addressed. Electronic mail: col@diam.unige.it

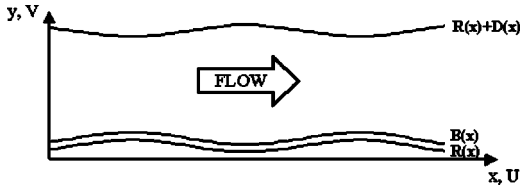

FIG. 1. Sketch of flow configuration.

sults of the decoupled analysis are briefly discussed and compared with experimental results in Sec. IV. The effect of coupling is discussed in Sec. V through a comparison of the behavior of the three eigenvalues that characterize the coupled solution with the corresponding decoupled eigenvalues. Some brief conclusions follow.

II. FORMULATION OF THE PROBLEM

Let us consider uniform turbulent free-surface flow of an incompressible fluid of density ρ in a wide straight channel. In the following, variables with a star superscript are to be intended as dimensional variables. A generic quantity has been made nondimensional using the friction velocity u_f^* and the depth D^* of the unperturbed uniform flow and the fluid density ρ. Moreover, we define the friction coefficient C assuming that, for uniform flow condition, the friction velocity u_f^* and the depth-averaged velocity U^* are related to the slope S and the Froude number Fr by the following law:

$$C = \frac{u_f^*}{U^*} = \frac{S^{1/2}}{\mathrm{Fr}}. \tag{1}$$

The unsteady Reynolds equations in dimensionless form are written as

$$U_{,t} + UU_{,x} + VU_{,y} + P_{,x} - 1 - T_{xx,x} - T_{xy,y} = 0, \tag{2a}$$

$$V_{,t} + UV_{,x} + VV_{,y} + P_{,y} + S^{-1} - T_{xy,x} - T_{yy,y} = 0, \tag{2b}$$

$$U_{,x} + V_{,y} = 0, \tag{2c}$$

where $\mathbf{U}=(U,V)$ is the local velocity vector averaged over turbulence, P is the mean pressure, and $\mathbf{T}=\{T_{ij}\}$ is the 2D Reynolds stress tensor.

Figure 1 shows a sketch of the flow domain referred to a Cartesian coordinate system (x,y). The flow is bounded by the curves $y=R(x,t)$ and $y=R(x,t)+D(x,t)$ in a way that D represents the local flow depth. The kinematic and dynamic boundary conditions to be associated with (2) then read

$$-R_{,t} + U_n = 0, \quad U_t = 0 \tag{3}$$

at the lower boundary, while at the upper boundary we have

$$-(R+D)_{,t} + U_n = 0, \quad \tau_t = 0, \quad \tau_n = 0, \tag{4}$$

where U_t and U_n are the tangential and normal components of velocity at the boundaries. In analogy, τ_t and τ_n are the tangential and normal components of the stress acting on each boundary. Furthermore, we set the lower boundary of the flow domain at a predefined reference level, which conventionally represents the zero-velocity plane for the logarithmic profile. If we denote by k_s the nondimensional roughness height and by κ the Kármán constant, set equal to 0.4, the law of the wall can be written as

$$U = \frac{1}{\kappa}\ln\left(\frac{y}{k_s}\right) + B_r = \frac{1}{\kappa}\ln\left(\frac{y}{y_r}\right), \tag{5}$$

where the constant B_r is commonly set equal to 8.5, which corresponds to a value of y_r of about $(1/30)$th of the roughness height. Typically, the latter is assumed to be around 2.5 times the grain size, leading to $y_r = d_s/12$, where d_s is the nondimensional sediment diameter. Moreover, the origin of the vertical axis is set at the average bed level, which falls at a distance of $d_s/6$ below the top of the grains.

A transformation of variables of the kind

$$\eta = \frac{y - R(\xi,\tau)}{D(\xi,\tau)}, \quad \xi = x, \quad \tau = t \tag{6}$$

is then employed to map the domain shown in Fig. 1 into a rectangular domain.

In order to close the above formulation a Boussinesq closure is used, which reads

$$T_{ij} = \nu_T(U_{i,j} + V_{j,i}). \tag{7}$$

The eddy viscosity ν_T has been evaluated by means of the mixing length approach

$$\nu_T = l^2 U_{,y} \quad l = DL(\eta), \tag{8}$$

where the algebraic function

$$L(\eta) = \kappa(\eta + \eta_r)(1-\eta)^{1/2} \tag{9}$$

produces, for a uniform flow, a parabolic profile of eddy viscosity and, consequently, the logarithmic law (5). Accordingly to the above considerations, the quantity η_r in (9) has been set to $d_s/12$.

As far as bed dynamics is concerned, only bedload transport is considered and the perturbation approach adopted by Colombini[8] to study dune and antidune formation in the decoupled framework is followed. It is convenient at this point to briefly summarize some of the salient concepts of this approach. For a more complete analysis the reader may refer to Ref. 8.

In the work of Bagnold,[15] which can be considered as the first mechanistic approach to sediment transport, "the rate of work done in pushing the bedload along the bed against frictional resistance" was related to "the power in the flow available to move the sediment," leading to a relationship between the sediment discharge per unit width and the bed shear stress. Most of the equilibrium relationship available in the literature for estimating the bedload transport intensity are based on the same approach, which can be essentially reduced to a force balance over a thin layer, often referred to as bedload or saltation layer, which bounds the region of fluid where sediments move by small jumps.

The clear fluid flowing above this bedload layer is practically unaffected by the sediment motion, which is felt by the fluid itself only as a slight change of roughness. Therefore, the shear stress acting on the top of the bedload layer can be assumed to be identical to that occurring, at the same

height above the reference level, in a uniform flow over a fixed bed characterized by the same roughness.

The thickness of the saltation layer scales with the sediment grain size d_s, e.g., is of the order of (1/100)th to (1/1000)th of the flow depth, and depends on the flow stage in terms of some power of the difference between the shear stress acting on the top of the bedload layer τ_b and the critical stress for sediment motion τ_c. We can then write

$$h_b = \left[1 + A_b \left(\frac{\tau_b - \tau_c}{\tau_c} \right)^m \right] d_s, \quad \tau_b \geqslant \tau_c, \tag{10}$$

where the value of the constant A_b and of the exponent m have been set equal to 1.13 and to 0.57, respectively, on the basis of a regression on experimental data.[8]

Due to the smallness of h_b, the difference in modulus between the shear stress τ_b and the shear stress evaluated at the reference level τ_r is quite small, so that apparently this difference can be ignored. However, the phase of the bed shear stress with respect to bed elevation, which plays a fundamental role in the stability process, varies quite rapidly in the neighborhood of the reference level and the resulting stability picture is significantly altered by this seemingly minor simplification.[8] Therefore, in the following we will keep distinct the reference level R, at which the boundary condition of vanishing velocity is set, from level B, at which the shear stress is evaluated in order to determine bed evolution. It is assumed that the two levels are kept at the same distance h_b as the bed evolves in time.

Based on the above considerations, the Exner equation of sediment mass conservation takes the form

$$B_{,t} = - Q_0 \Phi_{,x}, \tag{11}$$

where

$$Q_0 = \frac{\hat{Q}}{C(1 - \lambda_p)} \tag{12}$$

and

$$\hat{Q} = \frac{d_s^* \sqrt{(s-1) g d_s^*}}{D^* U^*} \tag{13}$$

is the ratio between the scale of sediment discharge and the flow rate; d_s^*, s, and λ_p are diameter, relative density, and porosity of the sediment, respectively, while g is gravitational acceleration.

Finally, in order to close the problem, a suitable relationship between the dimensionless sediment discharge per unit width

$$\Phi = \frac{q_s^*}{d_s^* \sqrt{(s-1) g d_s^*}} \tag{14}$$

and the flow must be introduced. Several formulations for the function Φ are available in the literature, all exhibiting a dependence by some power of a dimensionless form of the bed shear stress, known as the Shields stress θ_b.

$$\theta_b = \frac{\tau_b^*}{\rho (s-1) g d_s^*}. \tag{15}$$

Results of the linear stability theory are only moderately affected by the choice of a particular form of the function Φ. In the following, the Meyer–Peter and Müller formula

$$\Phi = 8(\theta_b - \theta_c)^{3/2} \tag{16}$$

has been employed, where θ_c is the critical Shields stress for incipient motion. When only bedload transport is considered, as in the present case, gravity favors the downhill motion of the grains and conversely opposes to the uphill motion. Following Fredsøe,[5] this effect has been accounted for setting the critical Shields stress θ_c to

$$\theta_c = \theta_{ch} - \mu (S - B_{,x}), \tag{17}$$

where θ_{ch} has been set equal to the conventional value for horizontal bed (0.047) and μ is a dimensionless constant that reads

$$\mu = \frac{\theta_{ch}}{\tan \Psi} \tag{18}$$

having denoted by Ψ the friction angle. An appropriate estimate for μ ranges[5] about 0.1.

III. LINEARIZATION

The problem formulated in the preceding section is then solved in terms of normal modes, so that a generic perturbed variable F can be written as

$$F(\xi, \eta, t) = F_0(\eta) + \epsilon F_1(\xi, \eta, t), \tag{19a}$$

$$F_1(\xi, \eta, t) = f(\eta) \exp[i\alpha(\xi - \Omega t)] + \text{c.c.}, \tag{19b}$$

where ϵ is a small parameter, α is the wave number of the perturbation, and Ω the complex growth rate.

By substituting the above expansion into the governing equations, boundary conditions, and turbulence closure, we are left with a sequence of problems at various orders of approximation in ϵ. In the following, we avoid the details of the above procedure and simply present its main results.

A. $O(\epsilon^0)$

At leading order, integration of the system of differential equations

$$T_{t0}' = -1, \quad T_{n0}' = - S^{-1}, \tag{20a}$$

$$T_{t0} = \nu_{T0} U_0', \quad T_{n0} = - P_0, \tag{20b}$$

where primes stand for $\partial / \partial \eta$ and

$$\nu_{T0} = \kappa (\eta_r + \eta)(1 - \eta) \tag{21}$$

together with the boundary conditions

$$U_0|_{\eta=0} = 0, \tag{22a}$$

$$T_{t0}|_{\eta=1} = 0, \quad T_{n0}|_{\eta=1} = 0, \tag{22b}$$

yield the classic rough logarithmic law for the velocity and the hydrostatic distribution for pressure

$$U_0 = \frac{1}{\kappa} \ln \left(\frac{\eta + \eta_r}{\eta_r} \right), \tag{23a}$$

$$P_0 = S^{-1}(1-\eta). \tag{23b}$$

Integrating once more the vertical profile of velocity, we obtain

$$\frac{U^*}{u_f^*} = \frac{1}{C} = \frac{1}{\kappa}\left[\ln\left(\frac{1+\eta_r}{\eta_r}\right) - 1\right], \tag{24}$$

which relates the friction coefficient C to η_r.

At the leading order, the Exner's equation (11) does not produce any additional information, since under uniform flow conditions the bed neither experiences aggradation nor degradation. It may just be worth mentioning the fact that

$$R_0 = \eta_0 = \frac{k_s}{30} = \frac{d_s}{12}, \quad B_0 - R_0 = \frac{d_s}{12} + h_b. \tag{25}$$

B. $O(\epsilon^1)$

We introduce two new variables to represent the amplitudes of the perturbed tangential stresses T_t and the perturbed normal stresses T_n with respect to a surface at constant η, which read

$$T_t = \nu_{T0}\left(u' - U_0' d + i\alpha v + \frac{\nu_T}{\nu_{T0}} U_0'\right), \tag{26a}$$

$$T_n = -p - 2i\alpha\nu_{T0} u, \tag{26b}$$

where u, v are the longitudinal and vertical components of the perturbed velocity, while p and d are the amplitudes of the pressure and flow depth perturbation, respectively. Finally, the mixing length formulation (8) allows us to write the ratio ν_T/ν_{T0} as follows:

$$\frac{\nu_T}{\nu_{T0}} = \frac{u'}{U_0'} + d. \tag{27}$$

After some manipulation a system of ordinary differential equations is eventually obtained that can be written in the general form

$$\mathcal{L}\mathbf{Z} = d\mathbf{D} + r\mathbf{R}, \tag{28}$$

where d is treated as a parameter to be determined and r is the amplitude of the perturbation of the reference level. The vector $\mathbf{Z}$ of the unknowns is

$$\mathbf{Z} = (u, v, T_t, T_n)^T. \tag{29}$$

The linear differential operator $\mathcal{L}$ in (28) reads

$$\mathcal{L} = \begin{pmatrix} d/d\eta & i\alpha/2 & -1/(2\nu_{T0}) & 0 \\ i\alpha & d/d\eta & 0 & 0 \\ A - 4\alpha^2\nu_{T0} & -U_0' & d/d\eta & i\alpha \\ 0 & A & i\alpha & d/d\eta \end{pmatrix}, \tag{30}$$

while the vector $\mathbf{D}$ and $\mathbf{R}$ are, respectively,

$$\mathbf{D} = \begin{pmatrix} 0 \\ i\alpha U_0'\eta \\ U_0' A\eta + i\alpha S^{-1}\eta - 2\alpha^2(1-\eta)\eta - 1 \\ S^{-1} + i\alpha\eta - 2i\alpha(1-\eta) \end{pmatrix} \tag{31}$$

and

$$\mathbf{R} = \begin{pmatrix} 0 \\ i\alpha U_0' \\ U_0' A + i\alpha S^{-1} - 2\alpha^2(1-\eta) \\ i\alpha \end{pmatrix}. \tag{32}$$

In the above relationships, the quantity A is equal to $-i(\alpha U_0 - \Omega)$.

Linearizing the boundary conditions (3) and (4) we obtain, at the reference level ($\eta = 0$)

$$u = 0, \quad v = -i\Omega r, \tag{33}$$

while at the free surface ($\eta = 1$)

$$v = i(\alpha U_0 - \Omega)(r + d), \quad T_t = 0, \quad T_n = 0. \tag{34}$$

The solution of the linear differential system (28) can be written in the form

$$\mathbf{Z} = c_1\mathbf{Z}_1 + c_2\mathbf{Z}_2 + d\mathbf{Z}_d + r\mathbf{Z}_r. \tag{35}$$

Thus $\mathbf{Z}$ is expressed as a linear combination of two linearly independent solutions of the homogeneous initial value problem, which satisfy the boundary conditions at the lower boundary

$$\mathcal{L}\mathbf{Z}_{1,2} = 0 \tag{36}$$

plus particular solutions of the nonhomogeneous differential systems

$$\mathcal{L}\mathbf{Z}_d = \mathbf{D}, \quad \mathcal{L}\mathbf{Z}_r = \mathbf{R} \tag{37}$$

again satisfying the lower boundary conditions.

Using the splitting (35) on the boundary conditions at the free surface (34), a set of three algebraic equations in the four unknowns c_1, c_2, d, and r is found, which, by replacing r with b, can be written as

$$\begin{pmatrix} a_{11} & a_{12} & a_{13} & a_{14} \\ a_{21} & a_{22} & a_{23} & a_{24} \\ a_{31} & a_{32} & a_{33} & a_{34} \end{pmatrix} \cdot \mathbf{X} = \begin{pmatrix} 0 \\ 0 \\ 0 \end{pmatrix}, \tag{38a}$$

where

$$\mathbf{X} = (c_1, c_2, d, b)^T. \tag{38b}$$

In obtaining (38), the two linearly independent solutions of the homogeneous problem (36) have been chosen so that the unknowns c_1 and c_2 are the values of the perturbation of the tangential and normal stress at the reference level, respectively. Furthermore, b is the amplitude of the perturbation of the surface B, which is identical to r since both B and R are proportional to the uniform sediment grain diameter and thus kept at a constant distance from one another as the bed evolves.

Linearization of the sediment continuity equation yields

$$\Omega b - Q_0 \alpha \phi = 0, \tag{39}$$

where the amplitude ϕ of the perturbation of the bedload discharge Φ defined by (16) can be expanded as in (35) leading to

$$\phi = (\phi_1 c_1 + \phi_2 c_2 + \phi_d d + \phi_b b) = \boldsymbol{\phi} \cdot \mathbf{X}, \tag{40}$$

where

$$\phi_1 = \left[\frac{\partial \Phi}{\partial c_1}\right]_0 = \left[\frac{\partial \Phi}{\partial \theta_b}\frac{\partial \theta_b}{\partial c_1} + \frac{\partial \Phi}{\partial \theta_c}\frac{\partial \theta_c}{\partial c_1}\right]_0 \tag{41}$$

and the suffix 0 stands for "evaluated at base condition." Analogous relationships hold for ϕ_2, ϕ_d, and ϕ_b.

Expanding also the perturbed shear stress T_{tb}, we then readily obtain

$$\boldsymbol{\phi} = A\left(T_{tb1}, T_{tb2}, T_{tbd} + \eta_b, T_{tbr} - i\alpha\frac{\mu}{\theta_{r0}}\right)^T, \tag{42}$$

where T_{tb1}, T_{tb2}, T_{tbd}, and T_{tbr} are evaluated at η_b and

$$A = \left[\frac{\partial \Phi}{\partial \theta_b}\right]_0 \theta_{r0}. \tag{43}$$

Making use of (40) and (42), we can rewrite (39) obtaining the dispersion relationship

$$\Omega b - Q_0 \alpha \boldsymbol{\phi} \cdot \mathbf{X} = 0. \tag{44}$$

Equation (44) provides the fourth equation to be associated with (38) so that a linear 4×4 algebraic homogeneous system is eventually obtained in the form

$$\mathbf{A}(\Omega) \cdot \mathbf{X} = 0. \tag{45}$$

The above system admits a nontrivial solution for the particular values of Ω that satisfy the eigenrelation

$$\det \mathbf{A} = 0. \tag{46}$$

The choice of different flow models (i.e., rotational vs irrotational flow) or the choice of coupling/decoupling flow and bed dynamics, only affect the values of the coefficients of the matrix $\mathbf{A}$, their dependence on Ω and the physical meaning of the constant c_1 and c_2. The mathematical asset of the problem remains unchanged and ultimately the eigenvalue problem described by (46) has to be solved.

IV. DISCUSSION OF RESULTS: DECOUPLED FLOW AND BED EIGENVALUES

A more detailed analysis of the eigenvalue problem (46) may help to enlighten the role of flow unsteadiness in the present problem and ultimately investigate the significance and well posedness of the hypothesis of decoupling flow and bed dynamics.

Let us write (45) as follows:

$$\begin{pmatrix} a_{11} & a_{12} & a_{13} & a_{14} \\ a_{21} & a_{22} & a_{23} & a_{24} \\ a_{31} & a_{32} & a_{33} & a_{34} \\ a_{41} & a_{42} & a_{43} & a_{44} \end{pmatrix} \cdot \begin{pmatrix} c_1 \\ c_2 \\ d \\ b \end{pmatrix} = \begin{pmatrix} 0 \\ 0 \\ 0 \\ 0 \end{pmatrix}. \tag{47}$$

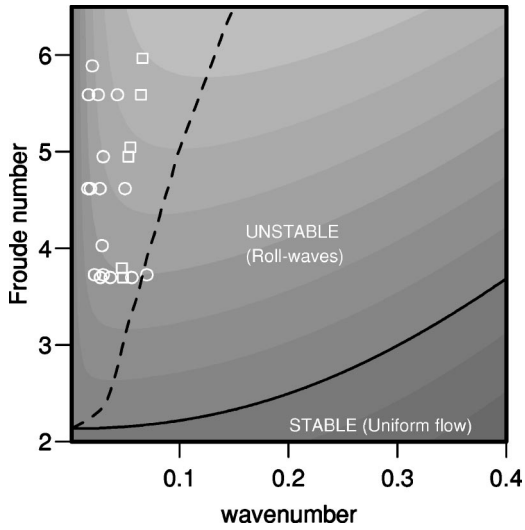

FIG. 2. Roll-wave instability: comparison with the experiments of Brock (Ref. 16): ○, finite amplitude roll waves; □, small amplitude roll waves.

If we now set $b=0$ and drop the last line of (47) (the Exner's equation) we obtain the eigensystem

$$\begin{pmatrix} a_{11} & a_{12} & a_{13} \\ a_{21} & a_{22} & a_{23} \\ a_{31} & a_{32} & a_{33} \end{pmatrix} \cdot \begin{pmatrix} c_1 \\ c_2 \\ d \end{pmatrix} = \begin{pmatrix} 0 \\ 0 \\ 0 \end{pmatrix}, \tag{48}$$

the solution of which provides the eigenvalues associated with the stability of a uniform flow over a flat, unerodible bed. Two eigenvalues are obtained, one associated to slower waves, always characterized by a negative growth rate, the other to faster waves that become unstable at high Froude numbers leading to roll-wave formation.

In Fig. 2 the stability diagram of the unstable eigenvalue is shown. In this and in all the subsequent stability plots, the complex quantity Ω has been rescaled with the uniform depth-averaged flow velocity U^* and its imaginary part has been multiplied by the wave number α to produce the growth rate, which is displayed in shades of gray, lighter colors corresponding to higher values. Moreover, the marginal (vanishing growth rate) curve is represented by a solid black line, while maximum growth rate is represented by a dashed black line.

This mode of instability is characterized by high wave celerities $[O(1)]$, large Froude numbers $(\mathrm{Fr} > 2)$ and small wave numbers. In the simulation, the value of the nondimensional roughness has been set equal to 0.0015, corresponding to a value of the friction coefficient $C=0.05$.

The experimental data of Brock[16] are also reported in Fig. 2. All the measured points follow in the unstable region and are characterized by wave numbers falling within a narrow band $(0 < \alpha < 0.06)$. The wave number of maximum amplification selected by the normal mode analysis seems to overestimate the experimental values. This discrepancy may be ascribed to the linearity of the present analysis, since nonlinear interactions have been shown to produce an increase in the wavelengths of roll waves as they reach finite amplitudes.[17] The wave numbers of small amplitude roll waves in the initial stage of development (shown as squares

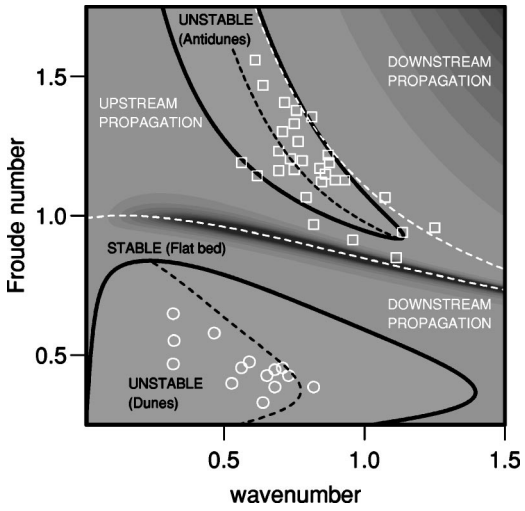

FIG. 3. Dune and antidune instability: comparison with the experiments of Guy, Simons, and Richardson (Ref. 21).

in Fig. 2) are closer to the line of maximum amplification than those of mature roll waves (shown as circles in the same figure).

Finally, the marginal curve and consequently the line of maximum amplification predicted by the present theory are found to be closer to the experimental points when compared to the results of existing shallow-water linear theories.[17–20] Therefore, the use of a more refined flow model is shown to improve the description of the instability process leading to roll-wave formation.

Bed-flow decoupling is obtained dropping time derivatives in the flow system (28) so that the coefficients of the first three rows of (47) are no longer functions of Ω. In this case the eigenrelationship (46) becomes linear and the (only) eigenvalue can be obtained solving first the linear algebraic system

$$\begin{pmatrix} a_{11} & a_{12} & a_{13} \\ a_{21} & a_{22} & a_{23} \\ a_{31} & a_{32} & a_{33} \end{pmatrix} \cdot \begin{pmatrix} c_1 \\ c_2 \\ d \end{pmatrix} = - \begin{pmatrix} a_{14} \\ a_{24} \\ a_{34} \end{pmatrix} b, \tag{49}$$

which provides the forced response of the flow to a bed perturbation of amplitude b, and second substituting the solution into (44). Most of the existing linear stability theories on bedform formation are based on the latter procedure, which dates back to the original work of Kennedy[1] and is often referred to as the "quasisteady hypothesis." This hypothesis relies on the fact that the ratio of the characteristic bed and flow time scales, i.e., $\hat{Q}$, is typically very small (e.g., of the order 10^{-3}).

The decoupled case has been extensively discussed in Colombini[8] and therefore only the comparison of the model results with the experimental measurements of Guy, Simons, and Richardson[21] is reported in Fig. 3 for completeness. The dashed white curves in the plot represent the lines of vanishing celerity.

The above formulation enlightens the real nature of the decoupling hypothesis: the coefficients of the two algebraic systems (48) and (49) coincide if one of the eigenvalues of the problem (48) is zero or, in other words, if perturbations of the flow do exist that are both neutral and stationary. If this is the case, a resonant problem is obtained since the system (49) is indeterminate producing an infinite response of the flow to bed perturbations and thus an infinite growth rate. This situation is exactly recovered only for the case of inviscid (irrotational) flow. However, when both celerity and growth rate of the slowest flow eigenvalue are small, the decoupled solution is strongly distorted by the quasiresonant behavior of the system, as it can be clearly seen in Fig. 3, where the artificial resonance introduced by the quasisteady hypothesis produces the dark region surrounding the dashed line of vanishing celerity.

We point out that the complete flow-bed system (47) does not exhibit any kind of resonance. Indeed, this is physically sound since no external forcing is present in this problem that could possibly lead to resonance if some natural response of the system were excited. The external forcing is artificially introduced when steady flow conditions are enforced according to the decoupling hypothesis.

V. DISCUSSION OF RESULTS: COUPLED FLOW AND BED EIGENVALUES

The procedure followed in the present work to solve the different eigenvalue problems which arise as particular cases of the complete eigensystem (45) is that described in Sec. III.

In particular, since the differential operator $\mathcal{L}$ parametrically depends on the complex growth rate Ω, each coefficient of the array $\mathbf{A}$ is in general a function of Ω and eventually three eigenvalues are found for any fixed value of the parameters. The search for the eigenvalues has been done numerically by means of a minimization of the determinant of the array $\mathbf{A}$, with an a posteriori check that an absolute minimum was actually found. The eigenvalues obtained by means of the decoupled flow and bed solutions were set as initial values of the above search procedure.

In the right column of Fig. 4, the three eigenvalues of the coupled solution are shown, while the corresponding eigenvalues of the decoupled solutions are reported in the left column. It may help the reader to recall at this point that the "flow-fastest" (a) and "flow-slowest" (c) eigenvalues follow from an analysis of flow instability over a flat fixed bed, while the "bed" eigenvalue (e) follows from the decoupled analysis of bed instability.

A comparison between the two lowermost rows of pictures in Figs. 4(c)–4(f) shows that the flow-slowest eigenvalue and the bed eigenvalue are clearly affected by the decoupling procedure. However, a distinction between flow and bed eigenvalues is no longer meaningful in the coupled case since they are just different eigenvalues of the unique flow-bed system. In particular, across the line describing steady flow perturbations the flow-slowest (d) and the bed (f) eigenvalues switch role, so that the unstable region associated with antidunes appears now in plot (d). It is important to note that the above mentioned deep valley associated to pseudoresonance disappears in the complete coupled solution, thus confirming that this effect is artificially introduced in the

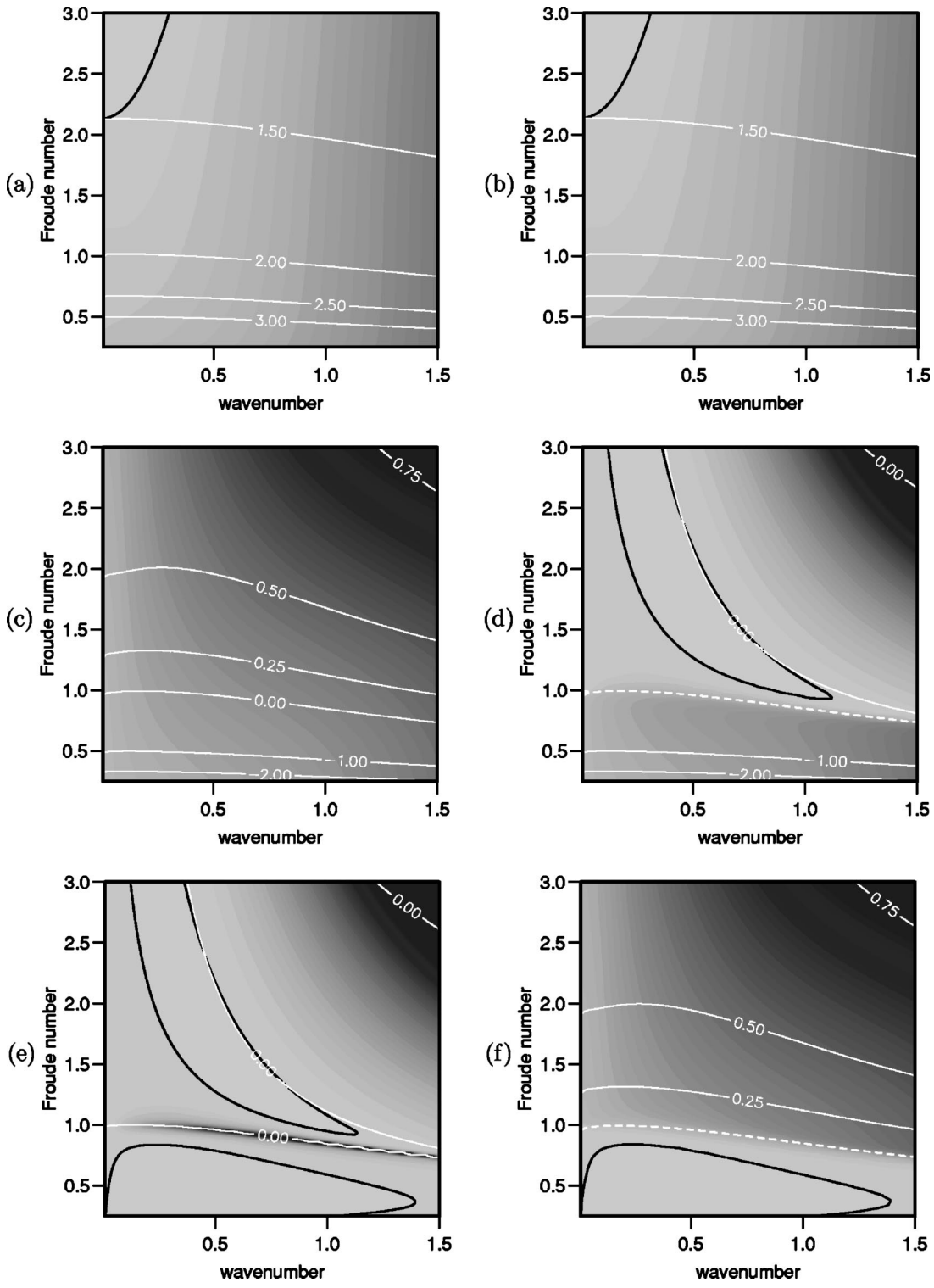

FIG. 4. Stability plot: comparison of decoupled (left column) and coupled (right column) solutions. The solid white curves are lines of equal celerity. The dashed white lines appearing in plots (d) and (f) represent steady flow disturbances.

analysis when the hypothesis of decoupling bed and flow dynamics is enforced.

In the framework of potential flow analyses, the resonance between bed and flow waves of the same celerity has been often invoked in the past as a possible instability mechanism.[10,22] Therefore, it may be worth to stress once more that a true resonance is obtained only if an external forcing excites some natural frequency of the system. The system at hand is a free oscillating system; it is the quasi-steady hypothesis that introduces an external forcing since steady flow disturbances resonate with the (almost steady) bed "forcing" configuration. When a coupled analysis is performed, independently from the flow model adopted, resonance in its commonly accepted meaning disappears so it can

be misleading to talk about the existence of a bed-wave-water-surface-wave resonance mechanism of instability.[10]

Indeed, in their potential flow coupled analysis, Coleman and Fenton[10] found instability for a narrow band of wave numbers falling in a neighborhood of the line describing steady flow perturbation. On the contrary, in the present rotational theory, the uniform flow is found to be stable in that region, in agreement with the experimental observations that the formation of dune and antidune occurs in subcritical and supercritical regimes, respectively, while a flat bed is observed for $\mathrm{Fr} \simeq 1$.[1,23]

Regardless the resonance problem, the marginal curves for dunes and antidunes appear to be practically unaffected by the coupling, thus suggesting that the dynamics of dune and antidune can be safely investigated in the simpler framework of the decoupled theory, at least for $\mathrm{Fr} < 2$.

As the Froude number increases above this threshold, in fact, also disturbances associated to the first eigenvalue become unstable [Fig. 4(b)], leading to the appearance of fast sediment waves that propagate downstream associated with the formation of roll waves. The existence of this mode of instability has been firstly discovered by Needham[12] using a coupled analysis based on a depth-averaged flow model. Due to the limitations of the shallow-water approach to small wave numbers, Needham[12] was unable to extend its analysis to cover also the case of dune and antidune formation, the characteristic wavelength of these bedforms scaling with the uniform flow depth. On the other hand, all the analyses based on the quasisteady approach clearly conceal the onset of sediment waves associated to the roll-wave formation. Present results confirm the appearance of fast-moving sediment waves at high Froude numbers, which are shown to coexist with slow-moving bedforms of the antidune kind in the same framework of analysis.

It may be useful at this point to briefly analyze the differences between these two modes of instability. In the following, we will refer to them as "antidune" and "roll-wave" modes for clarity. Antidune mode, as predicted by the present analysis, is characterized by a small negative celerity (upstream propagation), with a wavelength of maximum amplification that ranges from 5 to 20 times the averaged flow depth as the Froude number is increased. Roll-wave mode propagates downstream with an $O(1)$ celerity and is characterized by wavelengths larger than 30 times the uniform flow depth. Regarding the phase shift between the free surface and the bed oscillations, both antidunes and roll waves are approximately in phase, with a positive lag for antidunes, coherently with their upstream migration, and a negative lag for roll waves, corresponding to downstream migration.

Another distinctive feature of the two modes regard free-surface and bed oscillation amplitudes. As shown in Fig. 5, roll-wave disturbances are characterized by small ratio of bed over free-surface amplitude [e.g., $O(10^{-2})$]. On the contrary, the same ratio for antidunes is of the order 1. Results for roll-wave amplitude and phase lag are in qualitative agreement with the analysis of Needham.[14]

In summary, roll waves are therefore very long sediment waves, moving very fast and with very small bed amplitudes compared to the free-surface oscillations. They linearly compete, with similar growth rates, with antidunes, which are much shorter, slower, and characterized by larger bed amplitudes. Although in a linear context no further information is available on the competition of these two modes, the lack of experimental evidence of roll-wave sediment waves may be explained through the nonlinear competition with the antidune mode, which can possibly prevail on the other. Moreover, the present analysis suggests that if it is the roll-wave instability that eventually prevails, it may be easily confused with flat-bed conditions, since the amplitude of bed oscillations is small and their wavelength is large compared with antidunes.

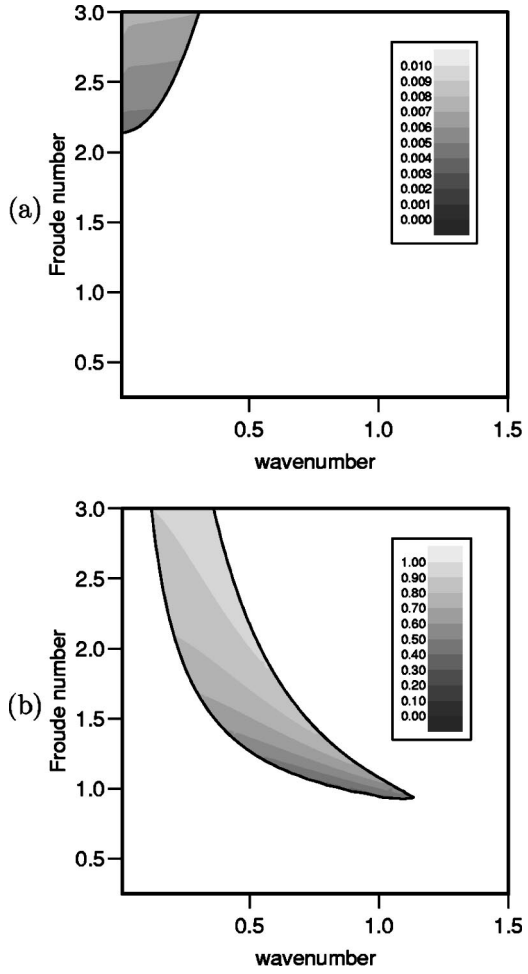

FIG. 5. Contours of the ratio of bed and free-surface amplitudes inside the regions of instability; (a) roll-wave mode, (b) antidune mode.

A fully or weakly nonlinear analysis of the process of instability that leads to the formation of roll waves and antidunes at high Froude numbers is required to shed some light on their reciprocal interactions.

VI. CONCLUSIONS

The present contribution deals with the linear stability of a uniform flow over an erodible bed in an infinitely wide open channel and, in particular, with the effect on the results of coupling or decoupling flow and bed dynamics.

The main conclusions can be summarized as follows:

(i) The coupled analysis leads to the same conclusions of the decoupled analysis as far as the regions of instability for dunes and antidunes are concerned.

(ii) The artificial resonance introduced in the decoupled analysis when the quasisteady hypothesis is enforced disappears when bed and flow dynamics are coupled together.

(iii) At high Froude numbers the existence of fast-moving sediment waves associated with roll-wave instability is found, confirming the results obtained in the framework of shallow water theories.

The roll-wave and antidune modes have been shown to be simultaneously unstable for sufficiently large values of the Froude number. No further information can be gathered, in a linear context, regarding their reciprocal interactions. An extension of the analysis to the weakly or fully nonlinear regime is required in order to provide a mechanism of competition between roll-waves and antidune modes, possibly leading to a transfer of energy between the two of them that can justify the dominance of one mode over the other.

ACKNOWLEDGMENTS

This research was partially supported by the Italian Ministero dell'Istruzione dell'Università e della Ricerca (Grants COFIN 2001 and COFIN 2003) and by the Fondazione Cassa di Risparmio di Verona, Vicenza, Belluno ed Ancona Project (RIMOF).

[1] J. F. Kennedy, "The mechanism of dunes and antidunes in erodible-bed channels," J. Fluid Mech. **16**, 521 (1963).
[2] J. F. Kennedy, "The formation of sediment ripples, dunes and antidunes," Annu. Rev. Fluid Mech. **1**, 147 (1969).
[3] F. Engelund, "Instability of erodible beds," J. Fluid Mech. **42**, 225 (1970).
[4] M. H. Gradowczyk, "Wave propagation and boundary instability in erodible-bed channels," J. Fluid Mech. **33**, 93 (1970).
[5] J. Fredsøe, "On the development of dunes in erodible channels," J. Fluid Mech. **64**, 1 (1974).
[6] F. Engelund and J. Fredsøe, "Sediment ripples and dunes," Annu. Rev. Fluid Mech. **14**, 13 (1982).
[7] B. M. Sumer and M. Bakioglu, "On the formation of ripples on an erodible bed," J. Fluid Mech. **144**, 177 (1984).
[8] M. Colombini, "Revisiting the linear theory of sand dune formation," J. Fluid Mech. **502**, 1 (2004).
[9] S. E. Coleman and B. W. Melville, "Bed-form development," J. Hydraul. Eng. **120**, 544 (1994).
[10] S. E. Coleman and J. D. Fenton, "Potential-flow instability theory and alluvial stream bed forms," J. Fluid Mech. **418**, 101 (2000).
[11] M. Colombini, G. Seminara, and M. Tubino, "Finite-amplitude alternate bars," J. Fluid Mech. **181**, 213 (1987).
[12] D. J. Needham, "The development of a bedform disturbance in an alluvial river or channel," ZAMP **39**, 28 (1988).
[13] R. Schielen, A. Doelman, and H. E. De Swart, "On the nonlinear dynamics of free bars in straight channels," J. Fluid Mech. **252**, 325 (1993).
[14] D. J. Needham, "Wave hierarchies in alluvial river flows," Geophys. Astrophys. Fluid Dyn. **51**, 167 (1990).
[15] R. A. Bagnold, "The flow of cohesionless grains in fluids," Philos. Trans. R. Soc. London, Ser. A **249**, 235 (1956).
[16] R. R. Brock, "Development of roll waves in open channels," Report. No. KH-R-16, California Institute of Technology, 1967.
[17] C. Kranenburg, "On the evolution of roll waves," J. Fluid Mech. **245**, 249 (1992).
[18] V. M. Ponce and D. B. Simons, "Shallow wave propagation in open channel flow," J. Hydraul. Div., Am. Soc. Civ. Eng. **103**, 1461 (1977).
[19] D. J. Needham and J. H. Merkin, "On roll waves down an open inclined channel," Proc. R. Soc. London, Ser. A **394**, 259 (1984).
[20] V. M. Ponce and M. P. Maisner, "Verification of theory of roll-wave formation," J. Hydraul. Eng. **119**, 768 (1993).
[21] H. P. Guy, D. B. Simons, and E. V. Richardson, "Summary of alluvial channel data from flume experiments 1956-61," U.S. Geol. Surv. Prof. Pap. **462-I**, 1 (1966).
[22] S. C. Jain and J. F. Kennedy, "The spectral evolution of sedimentary bed forms," J. Fluid Mech. **63**, 301 (1974).
[23] F. Engelund and J. Fredsøe, "Transition from dunes to plane bed in alluvial channels," *Inst. Hydrodyn. and Hydraulic Engng*, Series paper Vol. 4 (Tech. University Denmark, Lyngby, 1974).